Dynamics of the lowest-order bend-twist director mode near nematic–smectic-A criticality

H. K. M. Vithana, G. Xu, and D. L. Johnson
Department of Physics, Kent State University, Kent, Ohio 44242
(Received 23 November 1992)

A heterodyne light-scattering (LS) experiment that directly probes thermal fluctuations of the fundamental (lowest-order) bend director mode in homeotropic geometry, and a high-resolution Fréedericksz-transition (FT) experiment which excites the corresponding static mode magnetically were performed just above nematic–smetic-A criticality on the nonpolar wide-nematic-range material dihexylazoxybenzene over the reduced temperature ranges $3\times10^{-7}\le t\le2.0\times10^{-3}$ and $2.7\times10^{-5}\le t\le2.0\times10^{-2}$, respectively. It is found that over the nearly five decades of reduced temperature covered by these experiments, the enhancement of the bend elastic constant, K_{33}, obeys a simple power law with a critical exponent $\rho_3=0.825\pm0.008$ (FT), $\rho_3=0.815\pm0.03$ (LS); the error estimates include variations of ρ_3 upon extensive range shrinking and gap expansion of the data sets. These studies cover a wider range of reduced temperature and extend two decades or more closer to the critical point than previous studies. Over the nearly five decades of reduced temperature covered by these experiments the bend constant K_{33} increases by nearly four orders of magnitude to 5×10^{-3} dyn corresponding to a longitudinal correlation length of $\xi_\parallel=7.9t^{-0.82}$ Å ($\simeq200$ μm at $t=3\times10^{-7}$). The measurement of correlation lengths of this magnitude may be unprecedented in the study of critical phenomena. In spite of accessing the regime where $\xi_\parallel$ is comparable with the thickness of our films, ~200 μm, finite-size and surface effects are not observed. We also report the results of the above heterodyne experiment performed on another nonpolar material, hexyloxynonylbenzoate ($\bar{6}09$), over a similar reduced-temperature range. This experiment yielded the same critical exponent within experimental uncertainty, $\rho_3=0.84\pm0.03$, contrary to previously reported Fréedericksz-transition measurements which exhibited a crossover from ~0.84 to 0.67 on range shrinking and were well represented over the entire experimental range of reduced temperature by a power-law term with $\rho_3=0.67\pm0.02$ augmented by an anomalously large negative correction to scaling term. This discrepancy is discussed briefly in the context of surface phenomena and is currently under study. We compare our results with theoretical predictions about nematic–smectic-A criticality and with the director normal-mode spectrum which we derive from linearized Erickson-Leslie-Parodi theory including the effects of finite-director anchoring and surface dissipation.

PACS number(s): 64.70.Md, 64.60.Fr, 61.30.Cz

I. INTRODUCTION

After two decades of theoretical and experimental effort the nematic–smectic-A (N–Sm-A) phase transition remains a central unsolved problem of equilibrium statistical mechanics and eludes definitive experimental characterization. This is not to disclaim any success in understanding the problem; the predicted [1] Landau-Peierls instability of the smectic-A phase has been found experimentally [2] and the predicted thermal [3] and elastic constant [4] critical behavior is qualitatively correct. However, the critical exponents have been found not to be universal, although critical-to-tricritical crossover [5(a)] is a well-known complication and other effects such as strong but nondivergent enhancement of the splay elastic constant of weakly polar mesogens may also narrow the asymptotic regime [5(b)]. Therefore it is crucial, in our opinion, to probe critical fluctuations as close to the transition as possible.

In this article we present light-scattering and Fréedericksz-transition measurements of the bend elastic constant K_{33}, which collectively span nearly five decades of reduced temperature, $3\times10^{-7}<t<2\times10^{-2}$, and extend two decades closer to the transition than previous measurements of K_{33}.

The article is organized as follows. In Sec. II we derive the small-amplitude director normal-mode spectrum of a homeotropically aligned nematic from linearized Erickson-Leslie-Parodi hydrodynamic theory [6] including (1) a magnetic field perpendicular to the undistorted director, $\hat{\mathbf{n}}$, i.e., the bend Fréedericksz-transition geometry, (2) finite-director anchoring at the boundaries, and (3) *surface dissipation effects*. We find that the normal-mode spectrum has discrete wave-vector components parallel to $\hat{\mathbf{n}}$ which depend sensitively on the anchoring strength, the magnetic field, and bulk and surface coupling between the director field and the center of mass velocity field. In Sec. III we describe the bend Fréedericksz-transition and light-scattering experimental geometries and introduce the heterodyne correlation function for scattering from the fundamental director mode, the pure bend mode of lowest-allowed wave vector, i.e., the mode that is softened by the magnetic field at the Fréedericksz threshold. In Sec. IV we present our Fréedericksz-transition and light-scattering data, and derive from them the critical exponents ρ_3 for the materi-

als studied. We also discuss and summarize our results in the context of current theory and of other experiments.

II. DIRECTOR DYNAMICS: HOMEOTROPIC ALIGNMENT

The geometry of the normal modes of interest in our experiments is shown in Fig. 1. The small-amplitude director and velocity fields are

$$\hat{\mathbf{n}}=\hat{\mathbf{i}}n_x(y,z)+\hat{\mathbf{k}}=\hat{\mathbf{i}}\theta(y,z)+\hat{\mathbf{k}} \tag{1}$$

and

$$\mathbf{v}=\hat{\mathbf{i}}v_x(y,z)=\hat{\mathbf{i}}u(y,z)\ . \tag{2}$$

The fundamental assumptions about the dynamics of these fields are broken uniaxial symmetry, incompressibility, and negligible translational and rotational acceleration. The last two collectively assert that the nematic liquid crystal is a thoroughly overdamped system. All assumptions are supported by a variety of experimental results. The Erickson-Leslie-Parodi equations of motion for the mode-2 [7] (bend-twist) geometry arise directly from the vanishing of the gradient of the stress tensor and of the torque density; they are

$$\eta_a u_{yy}+\eta_c u_{zz}+\alpha_2\dot{\theta}_z=0\ , \tag{3}$$

$$K_{22}\theta_{yy}+K_{33}\theta_{zz}+\chi_a H^2\theta-\gamma_1\dot{\theta}-\alpha_2 u_z=0\ , \tag{4}$$

where $u_{yy}\equiv\partial^2 u/\partial y^2$, $\dot{\theta}\equiv\partial\theta/\partial t$, etc. The elasticity and viscosity coefficients are consistent with common notation; α_2 is the Leslie [6] viscositylike coefficient coupling director and center of mass motion and η_a,η_c are Miesowicz viscosities [8]. Note that all spatial variations are in the y-z plane, $\hat{\mathbf{n}}$ is in the x-z plane, and $\mathbf{H}=\hat{\mathbf{i}}H$; therefore we are considering only the mode-2 fluctuations maximally softened by the magnetic field.

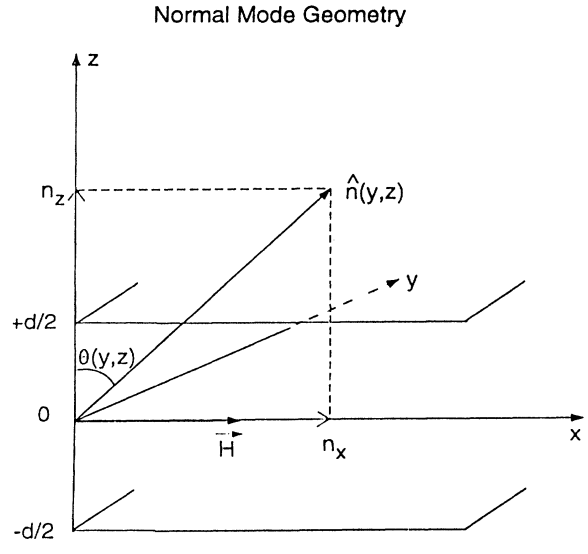

FIG. 1. Illustration of the coordinate system chosen for the analysis of the bend-twist normal-mode spectrum.

The question of boundary conditions is somewhat subtle. First we assume there is no flow at the boundaries, i.e.,

$$u(y,\pm d/2)=0 \tag{5}$$

and secondly that dissipation at the boundaries is finite as a result of finite-director anchoring; thus torque balance at the boundaries ($z=\pm d/2$) requires that

$$\gamma_{1s}\dot{\theta}(y,\pm d/2)+\alpha_{2s}u_z(y,\pm d/2) \pm K_{33}\theta_z(y,\pm d/2)+W_0\theta(y,\pm d/2)=0\ , \tag{6}$$

where γ_{1s} and α_{2s} are surface dissipation coefficients analogous to γ_1 and α_2, respectively, but with units differing by a factor of length, and W_0 is the anchoring energy coefficient. Thus director torques at the boundary in this model come from pure rotational friction (γ_{1s} term), coupling to shear flow (α_{2s} term), transmitted bend torque (K_{33} term), and surface reactive forces (W_0 term). We see that three surface-related coefficients are needed to describe the mode-2 director dynamics of this confined nematic liquid crystal, two of which (γ_{1s} and α_{2s}) we believe have not appeared in the literature. We have no *a priori* knowledge about the magnitude of the surface-dissipation coefficients but return to them in Sec. IV. If there were slip flow at the boundaries [$u(\pm d/2)\neq 0$] Eq. (5) would be replaced by $\eta_c\partial_z u(y,\pm d/2)+\alpha_2\dot{\theta}(y,\pm d/2)\pm\beta_s u(y,\pm d/2)=0$ leading to yet another surface friction coefficient, β_s. Equations (5) and (6) reduce to previously assumed boundary conditions [9] when surface dissipation is ignored.

Equations (3) and (4) have solutions of the form

$$\theta(y,z,t)=\theta(z)e^{iq_y y}e^{-t/\tau}\ , \tag{7}$$

$$u(y,z,t)=u(z)e^{iq_y y}e^{-t/\tau}\ , \tag{8}$$

which, upon substituting into Eqs. (3) and (4) yield

$$\eta_c u''(z)-\eta_a q_y^2 u(z)-(\alpha_2/\tau)\theta'(z)=0\ , \tag{9}$$

$$K_{33}\theta''(z)-(K_{22}q_y^2-\gamma_1/\tau-\chi_a H^2)\theta(z)-\alpha_2 u'(z)=0\ . \tag{10}$$

It is convenient to introduce the following definitions:

$$\rho\equiv\pi z/d\ , \tag{11a}$$

$$f(\rho)\equiv\theta(z)\ , \tag{11b}$$

$$g(\rho)\equiv(\pi\alpha_2\tau_0/\gamma_1 d)u(z)\ , \tag{11c}$$

$$\tau_0\equiv\gamma_1/K_{33}(\pi/d)^2\ , \tag{11d}$$

$$a\equiv(\eta_a/\eta_c)p^2\ , \tag{11e}$$

$$p\equiv q_y d/\pi\ , \tag{11f}$$

$$b\equiv(\alpha_2^2/\gamma_1\eta_c)\frac{\tau_0}{\tau}\ , \tag{11g}$$

$$h^2\equiv\chi_a H^2/K_{33}(\pi/d)^2\ , \tag{11h}$$

$$k_2\equiv K_{22}/K_{33}\ , \tag{11i}$$

$$c \equiv \frac{\tau_0}{\tau} - k_2 p^2 + h^2 \ . \tag{11j}$$

Then Eqs. (9) and (10) become, respectively,

$$g''(\rho) - a g(\rho) - b f'(\rho) = 0 \tag{12}$$

and

$$f''(\rho) + c f(\rho) - g'(\rho) = 0 \tag{13}$$

or more conveniently

$$f'''' + (c - a - b) f'' - acf = 0 \tag{14a}$$

and

$$g = a^{-1}[f''' + (c - b) f'] \ . \tag{14b}$$

The characteristic polynomial of Eq. (14a),

$$D^4 - (a + b - c) D^2 - ac = 0 \ , \tag{15}$$

has the four roots

$$2^{1/2} D = \pm \{ a + b - c \pm [(a + b - c)^2 + 4ac]^{1/2} \}^{1/2} \ . \tag{16}$$

Clearly if $c > 0$ (see below) two roots are real ($\pm R$) and two are imaginary ($\pm I$) and $f(\rho)$ is of the form

$$f(\rho) = A' e^{k\rho} + B' e^{-k\rho} + C' e^{iq\rho} + D' e^{-iq\rho} \ . \tag{17}$$

For g and f to be real we must have $C' = D'$ (real) or $C' = -D'$ (imaginary) and A' and B' must be real. Symmetry, or antisymmetry, about $\rho = 0$ then requires

$$f_E(\rho) = A \cosh(k\rho) + B \cos(q\rho) \tag{18}$$

or

$$f_O(\rho) = C \sinh(k\rho) + D \sin(q\rho) \ , \tag{19}$$

which describe even (E) and odd (O) director normal modes, respectively. The symmetry of the velocity field is opposite that of the director field as seen in Eq. (14b).

The dispersion relation analogous to that of the bulk nematic liquid crystal is then

$$t(z) \equiv \tau_0/\tau = \frac{(z^2 + k_2 p^2 - h^2)}{1 - z^2(\alpha_2^2/\gamma_1 \eta_c)/(z^2 + a)} \ , \tag{20}$$

where z can be q or ik and

$$k^2 - q^2 = a + b - c \ . \tag{21}$$

With Eqs. (20) and (11j) we may test $c > 0$,

$$c = \frac{q^2}{a + q^2(1 - x)} [q^2 + a + x(k_2 p^2 - h^2)] \ , \tag{22}$$

where

$$x \equiv \alpha_2^2/\gamma_1 \eta_c \ . \tag{23}$$

Now $0 \le x < 1$ is required for positive-entropy production and $h^2 < q^2$ is required for stability against a bend Fréedericksz distortion. Thus $c > 0$ is always true and our analysis above is valid for all allowed values of the physical parameters. An implication of this is that in semi-infinite geometry a homeotropically aligned nematic liquid crystal, unlike the case of homogeneous alignment, exhibits no surface modes although there may and, except for $p = 0$, will be deviations from bulk sinusoidal behavior near the surface, with k, the inverse decay length, given by Eq. (21). A complete treatment of both the even and odd modes under various assumptions about coefficients in the boundary conditions will be presented elsewhere [10]. Here our central interest is in the lowest-order even mode which we have studied by both light scattering and Fréedericksz transition.

The effect of the boundary conditions [Eqs. (5) and (6)] on the even modes is most easily discussed by rewriting Eq. (6) making use of Eqs. (11),

$$(W_0 - \gamma_{1s}/\tau) f(\pm\pi/2) + (\alpha_{2s}\gamma_1/\alpha_2\tau_0) g'(\pm\pi/2) \pm K_{33}(\pi/d) f'(\pm\pi/2) = 0 \ . \tag{24}$$

We introduce the length scale l,

$$l \equiv \gamma_{1s}/\gamma_1 \ , \tag{25a}$$

define

$$\nu \equiv \alpha_{2s}/\alpha_2 l \ , \tag{25b}$$

and eliminate the $g'(\pm\pi/2)$ term using Eq. (13) to get

$$\left[1 - d_e d_n \left[\frac{\tau_0}{\tau} - c\nu\right]\right] f(\pm\pi/2) + \nu d_e d_n f''(\pm\pi/2) \pm d_e f'(\pm\pi/2) = 0 \ , \tag{26}$$

where

$$d_e \equiv \frac{K_{33}\pi}{W_0 d} \tag{27}$$

is the extrapolation length (K_{33}/W_0) in units of d/π, and

$$d_n \equiv l\pi/d \tag{28}$$

is the new length scale in the same units. c is given in Eq. (11j) with the aid of Eqs. (20), (11d)–(11f), (11h), and (11i). For even modes Eq. (26) becomes

$$\left[1 - d_e d_n \left[\frac{\tau_0}{\tau} - c\nu\right]\right] f_E(\pi/2) + \nu d_e d_n f_E''(\pi/2) + d_e f_E'(\pi/2) = 0 \tag{29}$$

and substituting Eq. (18) into Eq. (29) gives

$$u(q) - u(ik) = 0 \tag{30}$$

and

$$A/B = -v(q)/v(ik) \ , \tag{31}$$

where

$$u(z) \equiv \frac{a + z^2}{z} \cot\left[\frac{\pi z}{2}\right] \times \{1 - d_e d_n [1 - t(z)(1 - \nu) + \nu(k_2 p^2 - h^2 + z^2)]\} - d_e z^2 \tag{32}$$

and

$$v(z)\equiv z\sin\left[\frac{\pi z}{2}\right]\Big/(a+z^2)\ . \tag{33}$$

Equations (20), (21), (30), and (31) along with the definitions of Eqs. (11a)–(11j), (25a), (25b), (27), (28), (32), and (33) are the central results needed to unravel the even-mode bend-twist fluctuation spectrum of a homeotropically aligned nematic. The material parameters entering these equations are K_{33}, K_{22}, W_0, χ_a, γ_1, l, ν, η_a/η_c, and $\alpha_2^2/\gamma_1\eta_c$.

Barring some unexpectedly strong mechanism for surface dissipation we will assume that l is approximately equal to the molecular length and $\nu\sim 1$. Since there are neither measurements of surface dissipation nor theoretical estimates of it, the above assumptions about it are the only currently reasonable ones. With these assumptions Eqs. (30) and (32) are replaced by

$$u_1(q)-u_1(ik)=0 \tag{34}$$

and

$$u_1(z)=\frac{(a+z^2)}{z}\cot\left[\frac{\pi z}{2}\right]\times[1-d_e d_n(z^2+k_2p^2-h^2)]-d_e z^2\ . \tag{35}$$

In our experimental geometry $p\sim 0$. In this limit Eq. (34) becomes

$$[1-d_e d_n(q^2-h^2)]\cot\frac{\pi q}{2}=d_e q+\frac{2\pi x}{q}\frac{(q^2-h^2)(1+d_e d_n h^2)}{q^2-xh^2}\ . \tag{36}$$

Now with l approximately equal to the molecular length (2.5×10^{-7} cm) and taking a realistic value for W_0 (~ 0.05 erg/cm^2) and K_3 ($\sim 10^{-6}$ dyn) and $d=200$ μm we have $d_e d_n\sim 3\times10^{-7}\ll 1$ which means that surface dissipation is unimportant under the above assumptions. Thus Eq. (36) becomes

$$\cot\frac{\pi q}{2}=d_e q+\frac{2\pi x}{q}\left[\frac{q^2-h^2}{q^2-xh^2}\right]\ , \tag{37}$$

which reduces, as required, to the Rapini-Papoular [11] form at the Fréedericksz transition ($h^2=q^2$). The lowest-q branch solution of $\cot\pi q/2=d_e q$ is relevant to our Fréedericksz-transition experiments whereas Eq. (37) with $h^2=0$, again the lowest branch of $\cot\pi q/2$,

$$\cot\frac{\pi q}{2}=d_e q+\frac{2\pi x}{q}\ , \tag{38}$$

is relevant to our light-scattering experiments. $2\pi x/q$ represents the role played by dissipation in determining the normal-mode fluctuation spectrum. $x=\alpha_2^2/\gamma_1\eta_c$, Eq. (23), is a measure of the coupling between shear flow and director rotation.

Eidner *et al.* [12] have studied the lowest even-order normal mode (the fundamental mode) in the presence of a magnetic field ($h^2<q^2$) using the same material and the same heterodyne experiment as the work reported here. They found that $t(q)$, the reduced decay rate [Eq. (20)] of this mode, decreases linearly toward zero, plotted against h^2, over the entire range of the experiment ($0\le h^2\le 0.94q^2$). The experiment was limited near $h^2=q^2$ by excessively long decay times. Such linearity of $t(q)$ vs h^2 can only occur when the $2\pi x/q$ term in Eq. (38) is negligible; then the light-scattering and Fréedericksz-transition data may both be analyzed with the $x=0$ version of Eq. (38); namely,

$$\cot\frac{\pi q}{2}=d_e q\ . \tag{39}$$

Thus, after all of the possibilities for deviant behavior presented by bulk and surface dissipation, the fundamental mode of this material, with the surface treatment used, behaves in the simplest way, i.e., according to the predictions of the static theory. Furthermore, it is demonstrated below that surface dissipation cannot enter because surface anchoring is always strong for our experiments; i.e., $d_e\sim 0$.

III. EXPERIMENT

A. Heterodyne light-scattering experiments

The geometry for this experiment is shown in Fig. 2; a discussion of it is given by Eidner *et al.* [12]. Light scattered by a pure bend mode exits the sample parallel to and negligibly displaced from the transmitted laser beam, independent of the angle of incidence; hence a homodyne experiment is impossible with real polarizers but the geometry is ideal for a heterodyne experiment.

The heterodyne autocorrelation function of interest here for photon arrivals at the photomultiplier tube (PMT) is

$$C(t)\equiv\langle n(0)n(t)\rangle=\langle n_{\rm LO}\rangle^2\left[1+\frac{2F(A)\langle n_s\rangle}{\langle n_{\rm LO}\rangle}e^{-t/\tau}\right]\ , \tag{40}$$

where $n(t)$ is the number of photons counted in a fixed time interval $\Delta t(\ll\tau)$ centered at t and includes both local-oscillator ($n_{\rm LO}$) and scattered-photon (n_s) contributions. $F(A)$ is a geometrical factor ranging from zero to one that measures the statistical coherence of the scattered light over the exposed area of the photocathode. $F(A)$ and the heterodyne efficiency should be near one for our geometry. Equation (40) leaves out the homodyne part of the autocorrelation function because in our experiments $\langle n_s\rangle\ll\langle n_{\rm LO}\rangle$ throughout the range of reduced temperature probed.

Figures 3 and 4 show two experimentally measured correlation functions; Fig. 3 was taken very near the transition temperature, $\log_{10}t=-6.35$, and Fig. 4 well above it, $\log_{10}t=-4.01$. The deviations from fitting these data to Eq. (40) are shown in the inset.

As can be seen in these figures the fits are excellent; the range of relaxation times encountered in these experi-

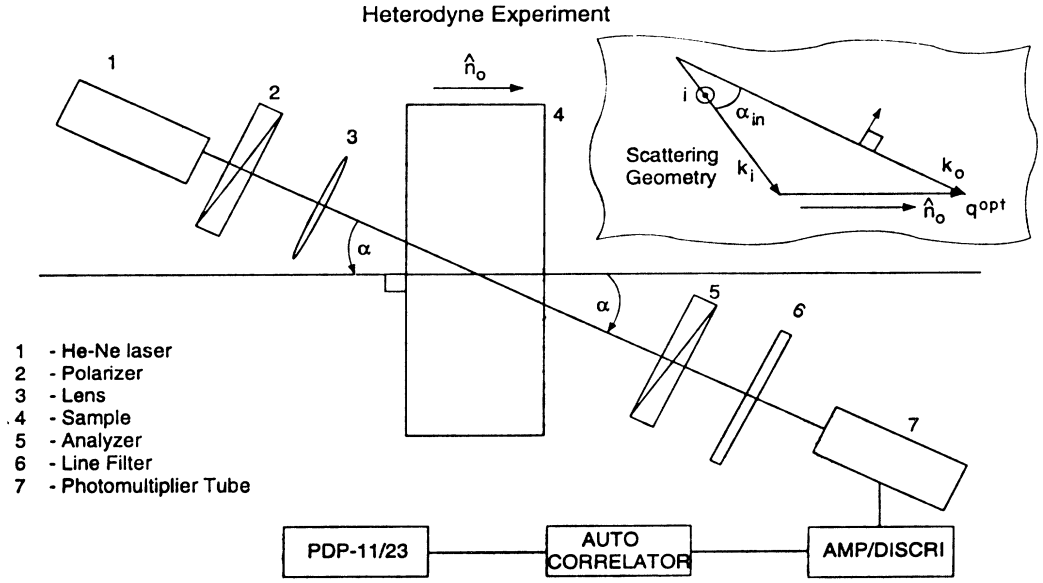

FIG. 2. Geometry of the heterodyne light-scattering experiment that detects the lowest even order normal mode (see text). α is the external incident angle used in calculating $\mathbf{q}^{\rm opt}$ using Eq. (41a); see the scattering diagram in the inset for the meaning of $\mathbf{q}^{\rm opt}$. $\hat{\mathbf{i}}$ and $\hat{\mathbf{f}}$ are the incident and scattered polarizations, respectively, and the scattering plane is also the plane of the rest of the figure.

ments is ~200 msec to 10 sec. The large magnitude of these relaxation times reflects the fact that we are observing very low-angle scattering. The components of wave-vector transfer parallel and perpendicular to the undistorted director are

$$q^{\rm opt}=q_{\parallel}^{\rm opt}$$

$$=k_v\left[\frac{n_o}{n_e}(n_e^2-\sin^2\alpha)^{1/2}-(n_o^2-\sin^2\alpha)^{1/2}\right] \tag{41a}$$

and

$$q_{\perp}^{\rm opt}=0\ , \tag{41b}$$

where $k_v=2\pi/\lambda_v$ (λ_v is the vacuum wavelength of He-Ne light, 6328 Å), n_e and n_o are the extraordinary and ordinary indices of refraction of the nematic dihexylazoxybenzene (DHAOB), and α is the external incident angle of the laser beam relative to the film normal. For both of the experiments reported here α is so small that $q_{\parallel}^{\rm opt}\leq\pi/d$. Therefore we are probing only the

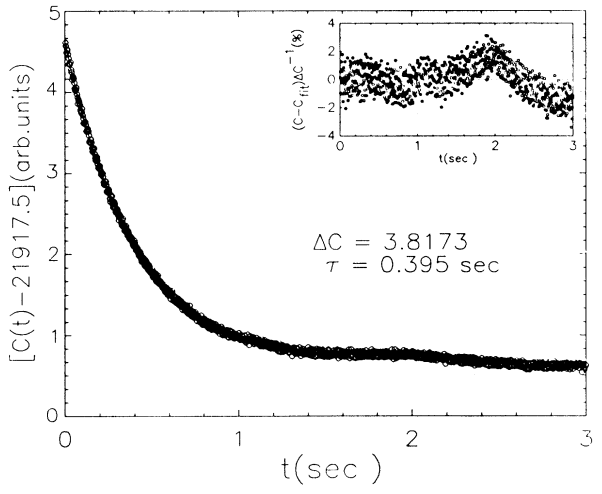

FIG. 3. Measured correlation function for $\log_{10}t=-6.35$. The inset is the deviation of the measured correlation function from the best fit to Eq. (40). The deviation is in units of the amplitude of the decaying part, i.e., $C(0)-C(\infty)$, and is expressed in percent. The graph represents 600 averages of a 1000 channel correlation function at 3 msec/channel.

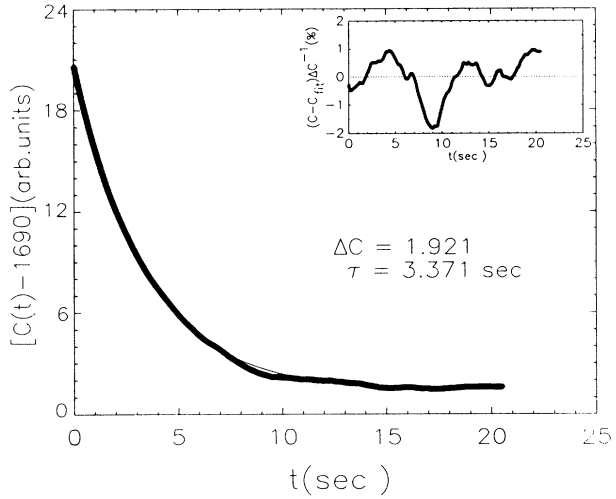

FIG. 4. Measured correlation function for $\log_{10}t=-4.01$. The inset is the deviation of the measured correlation function from the best fit to Eq. (40). The deviation is in units of the amplitude of the decaying part, i.e., $C(0)-C(\infty)$, and is expressed in percent. The graph represents 600 averages of a 1000 channel correlation function at 20.5 msec/channel.

lowest-order pure bend mode; this is actually a somewhat delicate point requiring further discussion.

The lowest-order normal mode is the lowest-branch solution of Eq. (38), or as we have pointed out in the preceding section, Eq. (39) for the experiments reported here. In the strong-anchoring limit ($d_e=0$) Eq. (39) gives $q=1$, i.e., the fundamental mode wave vector is $q_\parallel=\pi/d$; in the weak-anchoring limit ($d_e=\infty$) $q=q_\parallel=0$. Now $d_e=\pi K_{33}/W_0 d$ and K_{33} diverges as the smectic-A phase is approached; therefore it is not clear whether only the lowest-order normal mode is probed throughout the range of reduced temperature; furthermore, even if the fundamental mode is the only contributor of scattered photons it is not clear how much $q_\parallel$ may vary within its range $0\le q_\parallel\le\pi/d$. The next higher mode is an odd mode which we have not discussed here; however, we have examined it theoretically and it is just the lowest-branch solution of $-\tan\pi q/2=d_e q$, as in the static theory [12], under the same assumptions used in deriving Eq. (39). Thus if W_0 remained constant as K_{33} diverged this mode would tend to $q_\parallel=\pi/d$ while the fundamental mode goes to $q_\parallel=0$. For our experiments solutions of Eq. (41a) give $q_\parallel^{\rm opt}=\pi/d,\pi/3d$ for the two scattering angles studied; therefore it is clearly necessary to ask which modes are detected and how their wave vectors may change on approaching the smectic-A phase. Our experiments answer these questions.

The differential light-scattering cross section for a discrete bend mode of wave vector $q_\parallel$ is

$$\frac{d^2\sigma}{d\Omega d\omega}\sim\langle|n(q_\parallel)|^2\rangle\left[\frac{\sin(q_\parallel^{\rm opt}-q_\parallel)d/2}{(q_\parallel^{\rm opt}-q_\parallel)d/2}\right]^2\{\mathcal{R}\}\ , \tag{42}$$

where $\{\mathcal{R}\}$ is the appropriate selection rule [7] factor and the factor in square brackets is a single slitlike diffraction factor arising from interference due to the finite thickness of the sample,

$$\langle|n(q_\parallel)|^2\rangle=\frac{2k_BT/V_{\rm sc}}{K_{33}q_\parallel^2[1+\sin^2q_\parallel d/2q_\parallel d-x(\sin q_\parallel d/q_\parallel d)^2]} \tag{43}$$

for even modes [solutions of Eq. (38)] and

$$\langle|n(q_\parallel)|^2\rangle=\frac{2k_BT/V_{\rm sc}}{K_{33}q_\parallel^2\left[1+\sin2q_\parallel d/2q_\parallel d-\frac{\pi}{d_e}(\sin q_\parallel d/q_\parallel d)^2\right]} \tag{44}$$

for odd modes. $V_{\rm sc}$ is the scattering volume. Odd modes are solutions of

$$-\tan(q\pi/2)=d_e q\ . \tag{45}$$

The terms in the denominators of Eqs. (43) and (44) involving $\sin q_\parallel d$ and $\sin 2q_\parallel d$ reflect the cut off of z-axis integrations. The third term in the denominator of Eq. (43) is negligible since $x\ll1$ for DHAOB. The relaxation times for the pure bend normal modes probed here are given by Eq. (20) with $h=p=0$ and $x=0$; they are

$$\tau=\frac{\gamma_1}{K_{33}q_\parallel^2}\ , \tag{46}$$

where $q_\parallel$ is the solution of Eq. (39) or (45) for the lowest-

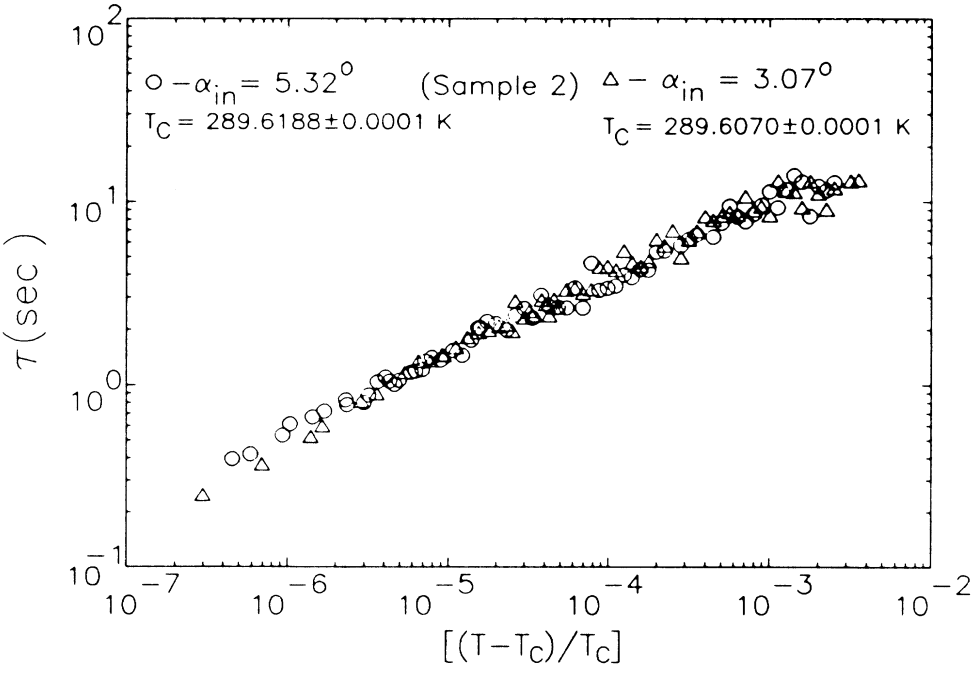

FIG. 5. Log-log graph of the relaxation time vs reduced temperature for the two scattering angles employed in the heterodyne experiment. $\alpha_{\rm in}=3.07°$ (5.32°) correspond to $q_\parallel^{\rm opt}=\pi/3d(\pi/d)$ where d is the sample thickness. $\alpha_{\rm in}$ and $q^{\rm opt}$ are defined by the inset of Fig. 2. The fact that $\tau(3.07°)=\tau(5.32°)$ throughout the range of reduced temperature probed to within experimental uncertainty is strong evidence that both experiments probe only the lowest-order even normal mode (see text).

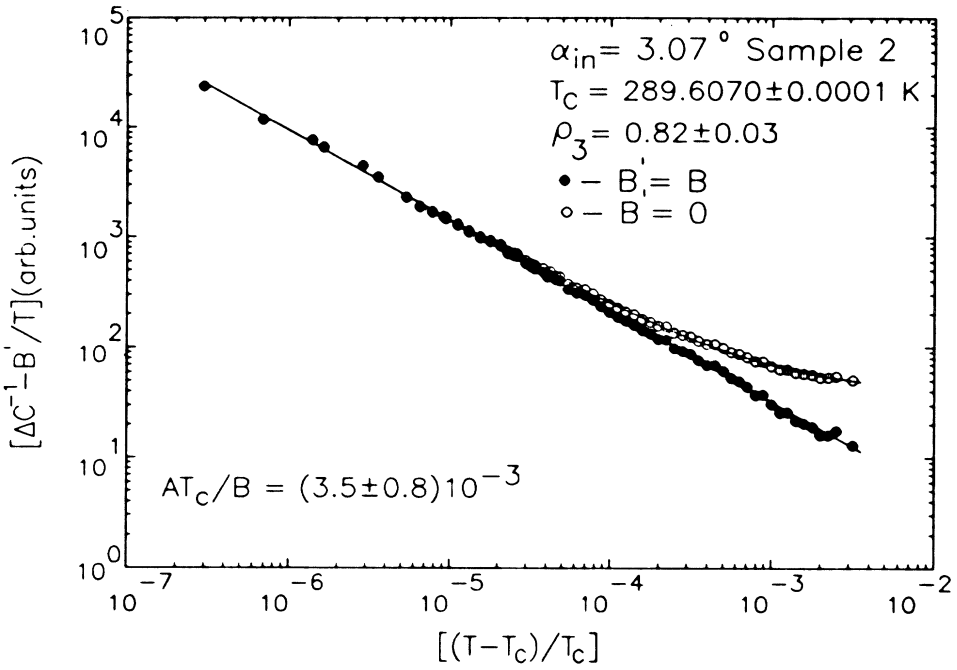

FIG. 6. Log-log graph of ΔC^{-1} (see text) vs reduced temperature with and without the background term, B/T, subtracted. ΔC^{-1} is a measure of the inverse of the scattering intensity; it is obtained by fitting measured correlation functions (e.g., Figs. 3 and 4) to Eq. (40). The solid lines are fits of ΔC^{-1} vs t to Eq. (48a). The best-fit values of T_c, ρ_3, and AT_c/B are given in the figure with their standard errors. AT_c/B is the ratio of the coefficients of the singular to the nonsingular parts of Eq. (48a) evaluated at T_c. The scattering angle for these data, $\alpha_{in}=3.07°$, is defined in Fig. 2.

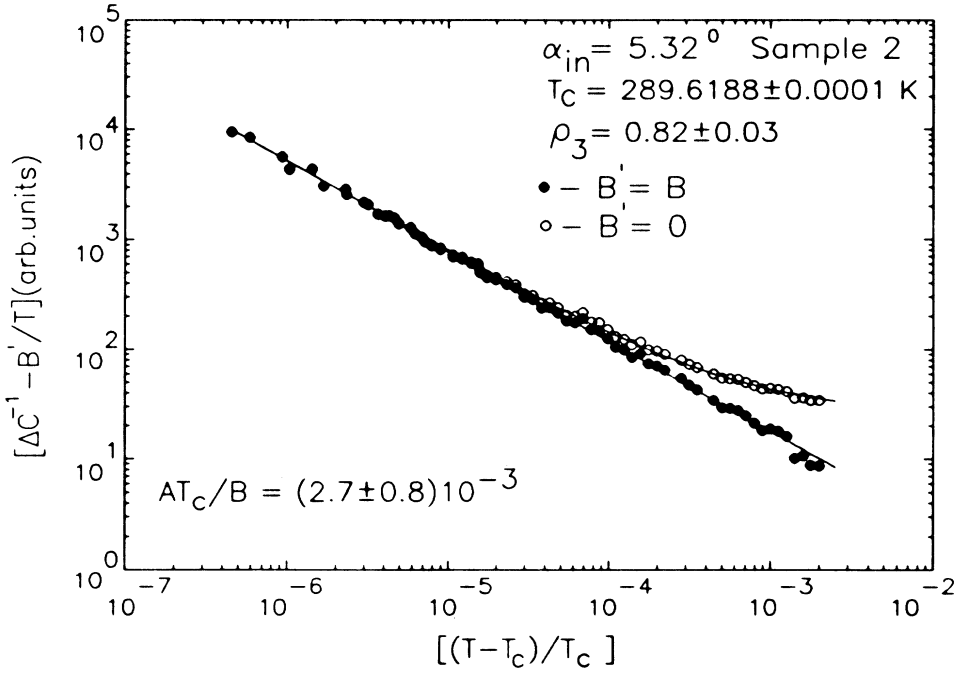

FIG. 7. Log-log graph of ΔC^{-1} (see text) vs reduced temperature with and without the background term, B/T, subtracted. ΔC^{-1} is a measure of the inverse of the scattering intensity; it is obtained by fitting measured correlation functions (e.g., Figs. 3 and 4) to Eq. (40). The solid lines are fits of ΔC^{-1} vs t to Eq. (48a). The best-fit values of T_c, ρ_3, and AT_c/B are given in the figure with their standard errors. AT_c/B is the ratio of the coefficient of the singular to the nonsingular part of Eq. (48a) evaluated at T_c. The scattering angle for these data, $\alpha_{in}=5.32°$, is defined in Fig. 2.

order even or odd mode, respectively.

The first evidence that our experiments probe only a single bend mode is that the single exponential form of Eq. (40) gives an excellent fit to all of the data at all temperatures and at both scattering angles; examples were given in Figs. 3 and 4. Secondly both experiments, i.e., both scattering angles, $q_{\parallel}^{\rm opt}=\pi/3d$ and π/d, yield the same relaxation times within experimental uncertainties over the entire range of reduced temperatures as shown in Fig. 5. Clearly the single slitlike diffraction factor in Eq. (42) significantly overlaps only one normal mode and it is the same normal mode for both experiments; furthermore, given the $q_{\parallel}^{\rm opt}$ values for these experiments, this must be the lowest-order normal mode, i.e., the lowest-branch solution of Eq. (39). Finally, that the wave vector of this mode is $q_{\parallel}\sim\pi/d$, i.e., that we are in the strong-anchoring regime, can also be deduced from Fig. 5. If strong anchoring were not present at low temperatures, e.g., if $d_e\equiv\pi K_{33}/W_0 d$ increases with K_{33}, an entirely reasonable possibility, the experiment done at $q_{\parallel}^{\rm opt}=\pi/d$ should begin to detect the first harmonic as the nematic–smectic-A transition is approached. Then, even if the ratio of first harmonic to fundamental scattering remained small enough that the single exponential form of Eq. (40) continued to give good fits, one would expect that the fitted values of τ from the $q_{\parallel}^{\rm opt}=\pi/d$ experiment would fall below those of the $q_{\parallel}^{\rm opt}=\pi/3d$ experiment as the transition is approached. Figure 5 shows that this is certainly not the case. We conclude that both experiments probe the lowest-order normal mode and that the wave vector of this mode is temperature independent and very near the strong-anchoring ($d_e=0$) solution of Eq. (39), namely, $q_{\parallel}=\pi/d$.

Since $q_{\parallel}=\pi/d$ is the only mode probed, the mean-square normal-mode amplitude [Eq. (43)] appropriate for the scattering cross section [Eq. (42)] is

$$\langle |n(q_{\parallel}=\pi/d)|^2\rangle=\frac{2k_BT}{V_{SC}K_{33}(\pi/d)^2}\ , \tag{47}$$

TABLE I. Results of fitting Eq. (48a) to the heterodyne light-scattering amplitude data as defined in Eqs. (48b) and (40). $\alpha_{\rm in}=3.07°$ (5.32°) is the internal scattering angle (see Fig. 2 inset) corresponding to $q_{\parallel}^{\rm opt}=\pi/3d(\pi/d)$; n is the number of data points removed from the data set to implement gap expansion (GE), see text. $t_{\rm min}(n)\equiv[T_{\rm min}(n)-\bar{T}_c(n)]/\bar{T}_c(n)$ where $T_{\rm min}(n)$ is the temperature of the data point nearest the N–Sm-A transition after n are removed, $\bar{T}_c(n)$ is the average of the fitted value of T_c over the entire range of range shrinking (RS), $t_{\rm max}^{l}<t_{\rm max}<t_{\rm max}^{u}$ where $t_{\rm max}^{l(u)}$ are the lower (upper) end of the reduced-temperature range spanned by RS and $t_{\rm max}\equiv[T_{\rm max}-\bar{T}_c(n)]/\bar{T}_c(n)$. For $\alpha_{\rm in}=3.07°$, $\log_{10}t_{\rm max}^{u}=-2.45$, $\log_{10}t_{\rm max}^{l}=-3.5$, $T_0=289.607$ K; whereas for $\alpha_{\rm in}=5.32°$, $\log_{10}t_{\rm max}^{u}=-2.60$, $\log_{10}t_{\rm max}^{l}=-3.5$, $T_0=289.6187$ K. The uncertainties in the fourth and sixth columns include not only the systematic variations of the fit parameters $T_c(n)$ and ρ_3 on RS but also their individual error bars. Systematic variations are in all cases comparable with parameter error bars which increase on RS. RS much deeper than $t_{\rm max}^{l}$ results in unacceptably large error bars and systematic variations.

$\alpha_{\rm in}$ (deg)	n	$\log_{10}t_{\rm min}^{(n)}$	$[\bar{T}_c(n)-T_0]$ (mK)	$\overline{\chi^2}$	$\overline{\rho_3}$
3.07	0	−6.63	0.01	0.70	0.820
			±0.04	±0.1	±0.03
	1	−6.24	0.025	0.70	0.820
			±0.04	±0.1	±0.03
	2	−5.95	0.07	0.65	0.808
			±0.07	±0.05	±0.03
	3	−5.88	0.085	0.65	0.805
			±0.08	±0.05	±0.03
	4	−5.64	0.16	0.6	0.79
			±0.09	±0.1	±0.03
	5	−5.48	0.07	0.6	0.81
			±0.16	±0.1	±0.04
5.32	0	−6.40	0.095	0.95	0.82
			±0.07	±0.1	±0.03
	1	−6.31	0.107	0.95	0.82
			±0.07	±0.1	±0.03
	2	−6.08	0.112	1.0	0.82
			±0.08	±0.1	±0.04
	3	−6.03	0.181	1.0	0.80
			±0.06	±0.1	±0.04
	4	−5.94	0.186	0.95	0.795
			±0.08	±0.1	±0.05
	5	−5.84	0.185	0.95	0.795
			±0.08	±0.1	±0.05

therefore, the temperature dependence of the coefficient of the exponential term in the heterodyne correlation function [Eq. (40)] is dominated by the temperature dependence of the bend coefficient, K_{33}.

To test the hypothesis that K_{33} exhibits a simple power-law divergence at the N–Sm-A transition we have fit the data to

$$\Delta C^{-1} = At^{-\rho_3} + \frac{B}{T} , \tag{48a}$$

where

$$\Delta C^{-1} \equiv [C(0) - C(\infty)]^{-1} . \tag{48b}$$

This form follows from the theoretical results of Jähnig and Brochard [13] who predict on the basis of de Gennes's model [1]

$$K_{33} = K_{30} + \delta K_3 , \tag{49a}$$

where

$$\delta K_3 = \frac{k_B T q_0^2}{24\pi} \xi_{\parallel} \tag{49b}$$

and

$$\xi_{\parallel} = \xi_{\parallel}^0 t^{-\rho_3} . \tag{49c}$$

They further suggest that three-dimensional (3D) XY critical exponents apply, as expected in a naive treatment of the de Gennes model [1] of the N–Sm-A transition where coupling between the director and smectic order parameter is not treated exactly.

The results of fitting both data sets to Eq. (48) are shown in Figs. 6 and 7. The fits are excellent ($\chi^2 \sim 1$) and the critical exponents are the same within experimental uncertainty, $\rho_3 = 0.815 \pm 0.03$, for both scattering angles.

We have analyzed these data in detail; the above error estimates include variations resulting from gap expansion (GE) and subsequent range shrinking (RS). GE means removing data point by point from the low-temperature end of the data set; we subsequently apply RS to the resulting data set. RS means removing data point by point from the high-temperature end of a given data set (after GE) and fitting the resulting data set to Eq. (48). The outcome of this data analysis is summarized in Table I.

B. Fréedericksz-transition experiments

The experimental geometry of the Fréedericksz-transition (FT) experiments is shown in Fig. 8. The photodiode detects the birefringence fringes that appear as the magnetic field is very slowly ramped through the critical field H_c. The photomultiplier tube detects light scattered from mode-2 director fluctuations with $q_{\parallel}/q_{\perp} \sim 10^{-3}$, i.e., nearly pure twist fluctuations; allowing us to monitor transition-temperature drifts (~ 1 mK/day) on a daily basis and to correct the temperature data correspondingly.

Due to finite magnetic-field ramp rates (~ 2.5 G/min) the onset and disappearance of fringes on increasing [$H_c(\uparrow)$] and decreasing [$H_c(\downarrow)$] field does not occur at the same field. $H_c(\uparrow) - H_c(\downarrow) \lesssim 40$ G throughout the range of temperatures probed and decreased upon approaching the N–Sm-A transition. We defined the measured critical field as the average of these, i.e., $H_c \equiv 1/2[H_c(\uparrow) + H_c(\downarrow)]$. Estimates of uncertainty in this H_c came from direct measurements of its reproduci-

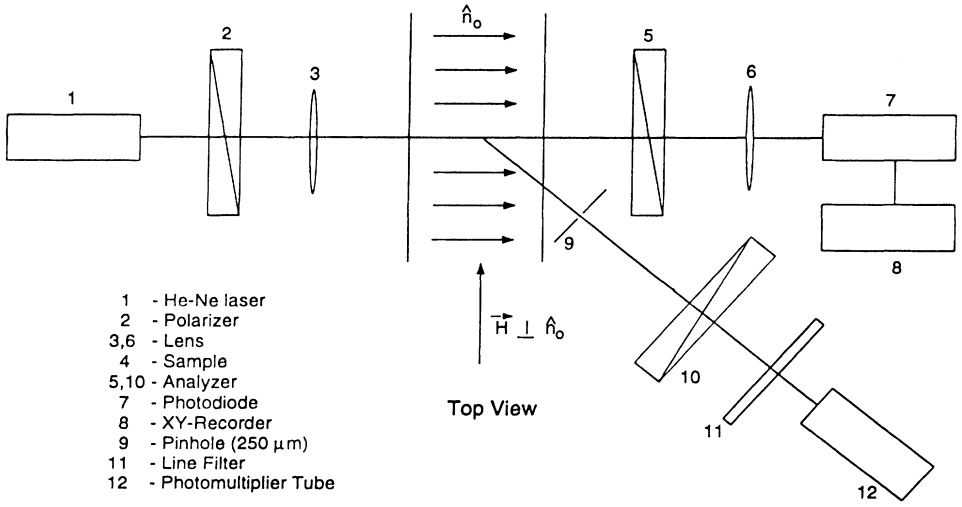

FIG. 8. Geometry of the bend Fréedericksz-transition experiment (transmitted light, 5–7 leg) and the nearly pure twist-mode auxiliary light-scattering experiment used to measure T_c drift with time (9–12 leg). For the FT experiment the polarizers (2 and 5) are crossed and at 45° to the plane of the figure. For the LS experiment polarizer 2 (10) is perpendicular (parallel) to the plane of the figure. The photomultiplier signal is delivered to a photon counting and autocorrelator system and the measured correlation function is fitted to an appropriate homodyne correlation function to get the amplitude (arbitrary units) and relaxation time of the nearly pure twist mode probed in this geometry. This auxiliary LS experiment is very similar to the one described in Ref. [4].

bility well above $T_{N\text{-Sm-}A}$ ($\sigma_H \sim \pm 2$ G) and from estimates of H_c drifts due to temperature drifts (± 50 μK), $\sigma_H = \sigma_T dH_c/dT$, which gave the dominant contribution very near $T_{N\text{-Sm-}A}$.

The above estimates of σ_H and the simple power-law form

$$H_c^2 = ATt^{-\rho_3} + B \tag{50}$$

gave an excellent statistical explanation of the data as evidenced by $\chi^2 \sim 1$ and the random appearance of deviations of the data from the best-fit functions (not shown). Our σ_H estimates were objective; therefore $\chi^2 \sim 1$ lends validity to Eq. (50) and allows us to estimate parameter uncertainties objectively. The results are shown in the log-log graphs of Figs. 9 and 10 where we have converted H_c^2 to K_{33} using Eq. (52) below and χ_a from the literature (see Sec. IV below). From Eqs. (49), we then have $A = (\pi k_B q_0^2/24\chi_a d^2)\xi_{\parallel}^0$ and $B = (\pi/d)^2 K_{30}/\chi_a$ where A and B are the coefficients in Eq. (50).

The simple power-law form is justified physically as follows. As noted in Sec. II the Fréedericksz transition occurs when $h = q$. The relevant wave vector is, therefore, the lowest-branch solution of Eq. (36) with $h = q$, namely,

$$\cot\frac{\pi q}{2} = d_e q \ . \tag{51}$$

This is the same as Eq. (39) except now it is exact for all values of the bulk and surface-dissipation coefficients, or equivalently x and d_n. This simplification illustrates the well-known fact that the wave vector at which a static thermodynamic instability occurs does not depend on dynamic properties. Thus Eq. (36) reduces, as required, to the Rapini-Papoular [11] result when $h \to q$. Of course, our conclusions in the preceding section still hold, namely, $q_{\parallel} = \pi/d$ (or $q = 1$) since we are in the strong-anchoring regime ($d_e = 0$). Hence we have

$$H_c^2 = \left[\frac{\pi}{d}\right]^2 \frac{K_{33}}{\chi_a} \ , \tag{52}$$

the usual bend-FT relationship; which, with Eq. (49), justifies Eq. (50).

As seen in Figs. 9 and 10 the FT data do not extend as close to T_c as the light-scattering (LS) data; specifically they terminate ~ 10 mK above T_c. This limit of our data occurs at the temperature below which the so-called stripe instability [14] is present. Although the stripe instability occurs above [15,16] the Fréedericksz field, H_c,

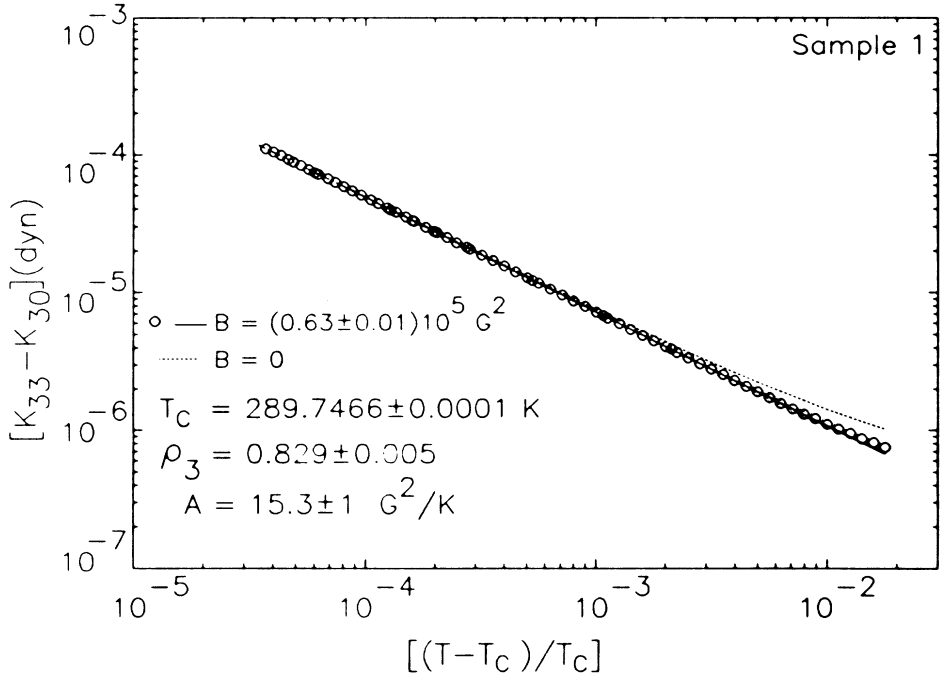

FIG. 9. Log-log graph of the bend elastic constant K_{33} vs reduced temperature $t \equiv (T - T_c)/T_c$ (T_c is the nematic–smectic-A transition temperature) with and without the background, $K_{30} = (\chi_a d^2/\pi^2)B$, subtracted, i.e., with $B = 0$ (upper curve) and $B = K_{30}$ (lower curve). Sample 1 is *not* the same sample studied in the light-scattering experiments. K_{33} was calculated from the measured (fitted) Fréedericksz fields, H_c, using Eq. (52) [Eq. (50)] and χ_a obtained from Ref. [17]. Therefore the solid lines are best fits of measured K_{33} to a simple power law in reduced temperature using Eqs. (50) and (52) as described in the text. The best-fit value of the H_c^2 [Eq. (50)] background B found from this fit is given in the figure and corresponds to $K_{30} = (3.49 \pm 0.07) \times 10^{-7}$ dyn, which is a very reasonable value. The best-fit values of the Eq. (50) critical exponent ρ_3, the amplitude A, and the critical temperature T_c are also given in the figure. At $t = 2 \times 10^{-2}$ this figure gives $K_{33} = 1.0 \times 10^{-6}$ dyn, which is within experimental uncertainty of the value obtained by de Jeu and Claussen [J. Chem. Phys. **67**, 3705 (1967)] at a similar reduced temperature using optical retardation vs field data beyond the FT in splay geometry to measure K_{11} and K_{33}/K_{11}.

it is very close to it and smears out the birefringence fringes, making it impossible to objectively determine H_c with sufficient accuracy. Note that the background contribution relative to the singular part is greater for the LS than for the FT data. This is due to the fact that focusing the laser beam to $b \sim 100\ \mu$m introduces uncertainty in $q_\perp$ of the order $2\pi/b$, thus bringing in contributions from splay and twist which only become negligible for $t \lesssim 10^{-5}$.

We have extensively analyzed the FT data using both the GE and RS procedures as with the LS data. Although the FT data do not extend as close to T_c as the LS data their scatter is much less, resulting in a very rigorous test of the acceptability of Eq. (50) as a parent distribution function. The results of this analysis are summarized in Table II.

It is of interest to compare $\overline{T_c}(n)$ with T_c derived from the auxiliary light-scattering intensity data collected in the T_c drift experiments discussed briefly at the beginning of this section. These scattering intensities were linearly extrapolated to zero to determine T_c; therefore they could not estimate T_c closer than ~ 1 mK, although their scatter was considerably less than 1 mK. $\overline{T_c}(n)$ for both samples and all n values differs by less than 1 mK from the values obtained from these auxiliary twist-mode light-scattering experiments.

The most striking outcome of our data analysis is the extreme stability of $\overline{T_c}(n)$ against both range shrinking and gap expansion in spite of the fact that the lowest-temperature data point is ~ 10 mK above T_c. RS of 0.75 decades and GE of ~ 0.5 decades leaves $\overline{T_c}(n)$ unchanged to within ± 0.1 mK for both samples. Extending GE to ~ 1 decade ($n = 26, 30$) and applying 0.75 decades of RS, which leaves < 20 data points at $t^l_{\max}$ (see Table I caption), results in $\lesssim 2$ mK shift of $\overline{T_c}(n)$ from $\overline{T_c}(0)$.

The stability of these fitted values of T_c against RS and GE and their excellent agreement with the light-scattering values, combined with the stability of fitted values of the exponent ρ_3 in the fifth column of Table II, provide strong empirical evidence supporting the simple power-law dependence of H_c^2 on reduced temperature and are rigorous confirmations of power-law behavior. We conclude that $\rho_3 = 0.825 \pm 0.008$ is a conservative statement about ρ_3 for DHAOB in the range $-4.5 < \log_{10} t < -2.0$ as Table II demonstrates.

The success of the FT and LS experiments depended on several factors. Submillikelvin temperature stability ($\lesssim 50\ \mu$K) was achieved through the use of an ac bridge, the heart of which is a seven-digit Gertsch ratio transformer (RT). The temperature coefficient of this cleverly

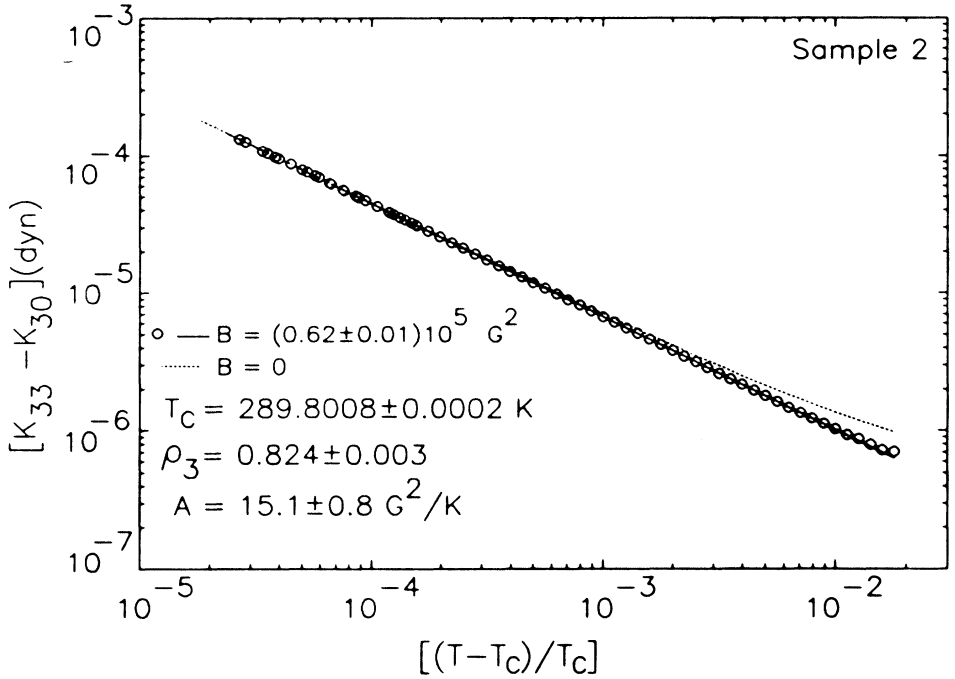

FIG. 10. Log-log graph of the bend elastic constant K_{33} vs reduced temperature $t \equiv (T - T_c)/T_c$, where T_c is the nematic–smectic-A transition temperature, with and without the background, $K_{30} = (\chi_a d^2/\pi^2)B$, subtracted, i.e., with $B = 0$ (upper curve) and $B = K_{30}$ (lower curve). Sample 2 is the same sample used in the LS experiments. K_{33} was calculated from the measured (fitted) FT fields, H_c, using Eq. (52) [Eq. (50)] and χ_a from Ref. [17]. Therefore the solid lines are best fits of measured K_{33} to a simple power law in reduced temperature using Eqs. (50) and (52) as described in the text. The best-fit value of the H_c^2 [Eq. (50)] background B found from this fit is given in the figure and corresponds to $K_{30} = (3.42 \pm 0.07) \times 10^{-7}$ dyn in excellent agreement with the value found for sample 1 (see Fig. 9 caption). The best-fit values of the Eq. (50) critical exponent ρ_3, the amplitude A, and the critical temperature T_c are also given in the figure. As for sample 1, there is good agreement with a literature value of K_{33} at $t = 2 \times 10^{-2}$ (see Fig. 9 caption).

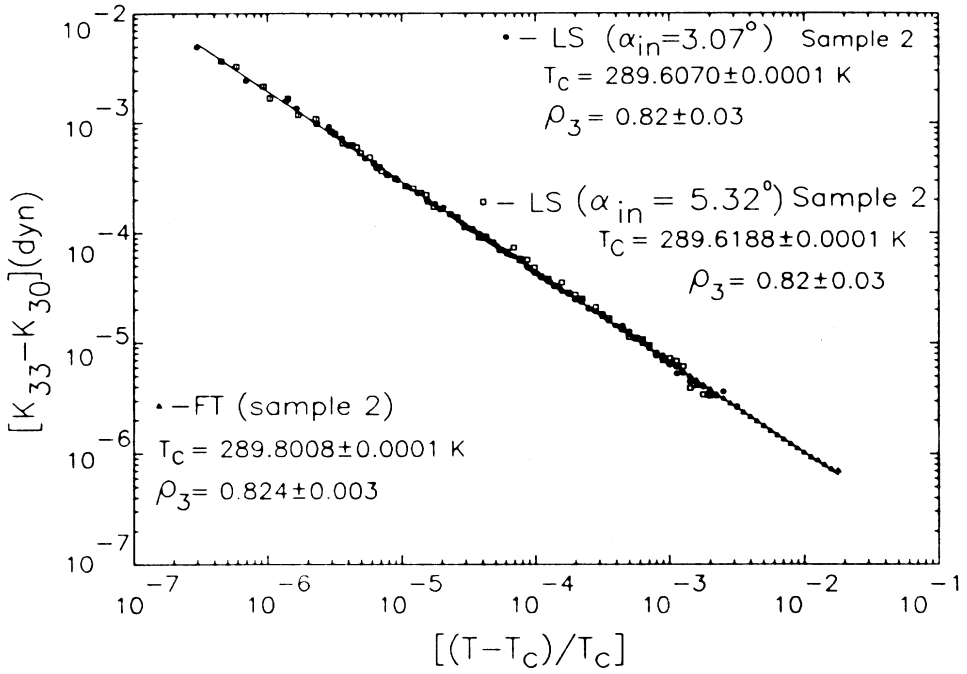

FIG. 11. Composite log-log plot of the singular part of K_{33} vs reduced temperature, including both LS and FT data. The LS data have been scaled on the vertical axis to match the FT data in the overlap region.

TABLE II. Results of fitting Eq. (50) to the Fréedericksz transition data for two samples of thickness $d=216$ μm. Sample 1 is the same sample as used in the light-scattering experiment. See the Table I caption for the definition of $t_{min}(n)$, $\overline{T_c}(n)$, $T_{min}(n)$, t^u_{max}, t^l_{max}, and T_0. For both samples $\log_{10}t^u_{max}=-2.00$ and $\log_{10}t^l_{max}=-2.75$. For sample 1 (2) $T_0=289.7466$ (289.8008). The discussion of parameter uncertainties given in the Table I caption applies here as well.

Sample	n	$\log_{10}t_{min}(n)$	$[\overline{T_c}(n)-T_0]$ (mK)	$\overline{\rho_3}$	$\overline{\chi^2}$
1	0	−4.43	0.00	0.828	1.0
			±0.14	±0.005	±0.10
1	1	−4.40	0.10	0.827	0.90
			±0.14	±0.005	±0.10
1	2	−4.37	0.07	0.827	0.90
			±0.17	±0.005	±0.10
1	3	−4.33	0.05	0.827	0.85
			±0.13	±0.005	±0.08
1	6	−4.24	−0.08	0.829	0.85
			±0.20	±0.005	±0.08
1	7	−4.22	−0.10	0.830	0.85
			±0.2	±0.005	±0.08
1	13	−4.02	−0.05	0.825	0.90
			±0.4	±0.01	±0.1
1	26	−3.60	−1.10	0.830	0.9
			±1.8	±0.015	±0.15
2	0	−4.57	0.00	0.824	0.9
			±0.06	±0.003	±0.10
2	1	−4.54	0.02	0.824	0.9
			±0.07	±0.003	±0.1
2	2	−4.47	0.02	0.823	0.95
			±0.08	±0.003	±0.08
2	3	−4.45	0.08	0.822	0.97
			±0.08	±0.003	±0.03
2	4	−4.42	0.12	0.821	0.97
			±0.08	±0.003	±0.03
2	17	−4.01	−0.08	0.833	0.40
			±0.5	±0.01	±0.05
2	30	−3.56	1.9	0.817	0.20
			±2.5	±0.015	±0.05

designed ac voltage divider is zero to first order because of intrinsic internal cancellations. We performed oven experiments which compare the output of RT's inside and outside the oven and could detect no difference in the seventh digit for temperature differences far in excess of those experienced in the laboratory. Our estimate of $\sim 50\ \mu$K is an upper limit on temperature stability based on the oven experiments. Window gradients were carefully studied [4] and are considerably less than 30 μK across the beam diameter; beam heating was negligible [4]. High-quality homeotropically aligned samples with no optically observable defects and very low T_c drift (~ 1 mK/day) were also essential as was the excellent reproducibility of our measurements of H_c as described above. Indeed, the scatter of the H_c^2 data is unobservable on the scale of the log-log plots of Figs. 9 and 10 in contrast with the light-scattering data which are intrinsically limited by photon statistics to much higher levels of scatter as shown in Figs. 6 and 7. The advantage of the heterodyne experiments is that they can be extended extremely close to T_c, approximately two decades closer than the FT data because the stripe phenomenon does not interfere.

Combined, these two experiments provide the most rigorous test to date of N–Sm-A criticality as characterized by power-law singularities. This is illustrated in Fig. 11, where we have plotted both FT and LS data. The LS data have been scaled vertically by a constant factor to agree with the FT data.

IV. DISCUSSION AND CONCLUSION

In Sec. II we derived the director normal-mode spectrum of a homeotropically aligned nematic liquid crystal from the Erickson-Leslie-Parodi hydrodynamic theory augmented to include finite-strength surface anchoring of the director and rotational and shear-flow surface-dissipation contributions to the orientational part of the entropy production. We restricted our attention to the bend-twist mode (mode 2) and included the effect of a symmetry breaking magnetic field in the bend Fréedericksz geometry, but only the case where the field is in the plane of the fluctuation. Generalization to arbitrary field orientation ($\mathbf{H}\perp\hat{\mathbf{n}}_0$) is straightforward and will be presented elsewhere [10]. Generalization to the bend-splay geometry is also straightforward but much more tedious and we have no plans at present to study it. We find no surface modes but do find additive nonsinusoidal ($\cosh kz$) contributions to the bulk modes. By comparing these theoretical results with heterodyne light-scattering relaxation-time experiments we were able to establish that these experiments probe only the lowest-order director mode and that the wave vector of this mode is temperature independent and very close to π/d, i.e., that strong anchoring applies throughout the range of reduced temperature of our experiments. Therefore, for our samples, we concluded that surface and bulk dissipation and finite anchoring do not affect the normal-mode spectrum, which is therefore composed of simple sinusoidal modes quantized in units of π/d in the $\hat{\mathbf{n}}_0$ direction. This further permitted us to conclude that the usual Fréedericksz transition relation, Eq. (52), applies.

Since light scattering at large scattering angle does not have the difficulties vis-à-vis the question of normal-mode structure that our experiment has it is useful to question why we have chosen to study the lowest-order mode. First of all it is the most sensitive probe of the effect of surface anchoring and dissipation, which are interesting in their own right; secondly it allows us to make direct connection and comparison with another important class of experiments, the FT experiments; and finally it does not have the problem of crossover into the nonhydrodynamic regime on approach to T_c suffered by high-q modes, until, of course, the smectic correlation length $\xi_\parallel$ becomes comparable with the film thickness, $d=216\ \mu$m, at which point one also expects the onset of finite-size and surface effects on the N–Sm-A transition. For the latter reason it is important to know whether $\xi_\parallel$ becomes $\sim d$ close to T_c in our light-scattering experiments; a point we return to after a discussion of the way we have determined $\xi_\parallel$ from our FT measurements.

Equations (49), (50), and (52) allow us to write

$$\xi_\parallel^0=\frac{24}{\pi}\frac{\chi_a}{k_B}\left[\frac{d}{q_0}\right]^2 A\ , \tag{53}$$

where $\xi_\parallel^0$ is defined in Eq. (49c) and is the so-called bare correlation length or correlation-length amplitude. All of the parameters on the right-hand side of Eq. (53) are known quite accurately. Specifically $\chi_a=1.1\times10^{-7}$ emu [17], $d=216\pm2\ \mu$m, and $q_0=0.234\ (\text{Å})^{-1}=2\pi/l$ where l is the extended molecular length, and $A=15.2\ \text{G}^2\ \text{K}^{-1}$ from our present results. This leads to $\xi_\parallel^0=7.9$ Å, which is slightly less than one-third of a molecular length; of course, $\xi_\parallel$ has no direct physical meaning on the molecular scale of lengths. This estimate of the bare correlation length is quite accurate (±0.5 Å) but its physical meaning is in some doubt because Eq. (53) relies on Eq. (49b), which is a result of a mean-field calculation by Jähnig and Brochard that may not be applicable in the critical regime. If we use this value of $\xi_\parallel^0$ to calculate the smectic correlation length at the low end of the reduced-temperature range spanned by our light-scattering data we find $\xi_\parallel(3\times10^{-7})=190\ \mu$m, which is very close to the film thickness $d=216\ \mu$m. We stress that this is an enormous correlation length, possibly among the largest ever measured near a phase transition of any kind, if indeed the Jähnig-Brochard calculation is correct as to order of magnitude of $\xi_\parallel^0$ which, as we shall show, it probably is. We note that this correlation length is derived from an elastic property, not from x-ray scattering; the latter detects the growth of smectic fluctuations. In this regard we would comment that our bare length and critical exponent for $\xi_\parallel$ are comparable with those found by x-ray scattering for several nonpolar materials, however, x-ray experiments are resolution limited to $t\gtrsim3\times10^{-5}$, two orders of magnitude further from T_c than our experiments. Recent results on a mixture of DHAOB (C_6) and 10% of its neighboring homolog, di-heptylazoxybenzene (C_7),

yield a smaller critical exponent [18] ($\nu_{\parallel}=0.75\pm0.03$) and bare length ($\xi_{\parallel}^{0}=7.2$ Å, no uncertainties given), a rather surprising result in light of the good agreement between elastic constant and x-ray scattering measurements of $\xi_{\parallel}$ found for a number of materials by Sprunt, Solomon, and Litster [19]. The results of Ref. [19] strongly suggest that our calculated $\xi_{\parallel}$ should be a good measure of the extent of smectic fluctuations in the direction of $\hat{\mathbf{n}}_0$. Therefore the disagreement between our results and the x-ray results on the $C_6(90\%)$-$C_7(10\%)$ mixture is all the more puzzling. Recent birefringence measurements [20] on the alkylazoxybenzene series have located a tricritical N–Sm-A point (TCP) at $\sim C_7(50\%)$-$C_8(50\%)$. The nematic range at the tricritical point, measured by $t_{IA}\equiv(T_{NI}-T_{N\text{-Sm-}A})/T_{NI}$, is $t_{IA}^{TC}=0.023$ whereas $t_{IA}(C_6)\sim t_{IA}(C_6(90\%)\text{-}C_7(10\%))\sim 0.115$. Hence both C_6 and $C_6(90\%)$-$C_7(10\%)$ are very far, and equally far, from the TCP by this measure, deepening the mystery about their different $\xi_{\parallel}$'s. We do not understand this clear-cut disagreement [21]. It flies in the face of the extensive studies of Ref. [19] and of our current level of understanding of N–Sm-A tricriticality. If the observed difference in $\xi_{\parallel}$ is material related, the chemical difference, or physicochemical difference of importance is not reflected in the nematic range parameter t_{IA}.

There is another puzzling feature of these results. Our own earlier FT studies [15] of three nonpolar systems with $t_{IA}\sim 0.06$ found a crossover of ρ_3 from values comparable to that reported here to much lower values, close to the three-dimensional (3D) XY prediction ($\sim\frac{2}{3}$). Adding a very large and negative correction to scaling term to the power law resulted in excellent fits over the entire range of reduced temperature probed, critical temperatures very close (~ 1 mK) to those obtained from the auxiliary light-scattering experiments, and exponents $\rho_3=0.67\pm0.02$ for all three materials. It is difficult to reconcile such behavior with that reported here for DHAOB, $\rho_3=0.825\pm0.008$. Crossover from tricritical to critical is superficially inconsistent with the expectation that tricritical exponents are smaller than critical exponents; however, exponent crossover need not necessarily be monotonic. If $\rho_3=0.825$ represents some intermediate crossover regime, and ρ_3 is near a peak, it is curious that this regime is more stretched out for DHAOB, with $t_{IA}=0.115$, than for the other three materials for which $t_{IA}\sim 0.06$, and which therefore are presumably closer to a TCP than DHAOB. In other words, this explanation would require the asymptotic critical regime of the three materials situated closer to the TCP, as measured by t_{IA}, to be much broader than for DHAOB which is much further from the TCP; not impossible but unusual by naive considerations. We cannot convincingly explain the physical origin of this difference of behavior, but it is important to note that there was another experimental feature of the previous work [15] that we could not then and cannot now satisfactorily explain. All three of the materials exhibited a very small but measurable dependence of T_c on applied magnetic field, $T_c(H)$; it was measured by monitoring the onset of light scattering on warming through T_c in the presence of a bend Fréedericksz geometry field. Although T_c only increased by a few mK at the largest Fréedericksz fields employed it was necessary to make corrections to the FT temperature data in order to gain agreement between the fitted T_c's and the auxiliary light-scattering T_c's.

To learn whether the $T_c(H)$ and ρ_3 crossover phenomena are related we performed the heterodyne light-scattering experiment on one of the three materials studied by FT earlier and which exhibited $T_c(H)$ and ρ_3 crossover, namely, hexyloxythiobenzoate ($\bar{6}09$). We found $\rho_3=0.844\pm0.035$ and *no crossover* to the lower value ($\sim\frac{2}{3}$) even though the data extended to $t=6\times10^{-7}$, nearly two decades closer to T_c than the earlier FT data [22]. Furthermore, this $\bar{6}09$ sample did not exhibit the $T_c(H)$ phenomenon, suggesting that $T_c(H)$ and ρ_3 crossover are related experimental artifacts. We now interpret the earlier data [15] differently and place more trust in the values obtained from the simple power-law fits reported there even though the χ^2 values were quite large as a result of the high precision of the FT experiments. Our best estimates are $\rho_3=0.82\pm0.04$ for all three of these materials, $\bar{6}09$, octyloxythiolbenzoate ($\bar{8}$S5), and nonylthiolbenzoate (9S5); consistent with x-ray scattering measurements [23,24] which, however, do not exist for 9S5. It therefore now appears that $\rho_3\sim 0.82$ for nonpolar materials with wide nematic ranges. Finally we can say that for DHAOB $\rho_3=0.825\pm0.008$ in the range $-4.5<\log_{10}t<-2.0$ and that any deviations from pure power-law behavior are small indeed; furthermore, any crossover to another regime in the range probed by our heterodyne experiments ($-6.5\lesssim\log_{10}t\lesssim-3.0$) must involve changes in ρ_3 smaller than approximately ±0.03.

Earlier light-scattering studies of twist-mode fluctuations of DHAOB gave $\rho_2=0.67\pm0.02$, in a comparable range of reduced temperatures ($-6.5<\log_{10}t<-3.0$), allowing us to extract the anisotropy of the thermodynamic correlation-length exponents by comparison with our current work. This anisotropy is given by $(\rho_3-\rho_2)/2=0.078$ which is rather small by comparison with narrower-nematic-range nonpolar materials, consistent with earlier findings and contrary to all theoretical results. We believe this to be a rigorous test of correlation-length exponent anisotropy.

Intriguing questions remain related to the curious $T_c(H)$ phenomenon and its companion ρ_3 crossover observed in three nonpolar materials but not in DHAOB. We do not understand this but one clue is that it does not always happen as our experience with $\bar{6}09$ proves. The agreement between our LS and FT results for DHAOB suggests that these phenomena are not due to the softening of rigidly anchored bend modes as a result of the applied field. We do not believe that sample impurities are responsible for the $T_c(H)$ and ρ_3 crossover phenomena because of the very similar behavior (identical correction to scaling terms) exhibited by the three quite different materials. The only remaining possibility appears to be that $T_c(H)$ and ρ_3 crossover are related to surface-anchoring or surface-ordering phenomena. Finally, we believe that a related question is raised by the experimental fact that for DHAOB the quantity $d_e\equiv\pi K_3/W_0 d$

does not appear to diverge. We note that $d_e \gtrsim 0.1$ would lead to observable (but unobserved) weak anchoring near T_c. Typical values of W_0 would give $d_e \sim 10$ at $t \sim 3 \times 10^{-7}$. It seems clear that W_0 must increase to values much larger than those typically observed in normal nematics liquid crystals away from smectic transitions [25]. Again surface phenomena appear to be crucial but not understood. We are currently pursuing these questions.

ACKNOWLEDGMENT

The authors acknowledge support for this research from the National Science Foundation's Advanced Liquid Crystalline Optical Materials (ALCOM) Science and Technology Center under Grant No. DMR-8920147.

[1] P. G. de Gennes, J. Phys (Paris) Colloq. **4**, C4-65 (1969); Solid State Commun. **10**, 753 (1972).

[2] J. Als-Nielsen, R. J. Birgeneau, M. Kaplan, J. D. Litster, and C. Safinya, Phys. Rev. Lett. **39**, 1668 (1977); J. Als-Nielsen, J. D. Litster, R. J. Birgeneau, M. Kaplan, C. R. Safinya, A. Lindegaard Andersen, and S. Mathiesen, Phys. Rev. B **22**, 312 (1980).

[3] C. W. Garland, G. Nounesis, M. J. Young, and R. J. Birgeneau, Phys. Rev. E **47**, 1918 (1993), and references therein. This is a review of specific heat and x-ray data and includes new x-ray data; it makes a case for the agreement of correlation volume, susceptibility, and specific heat data with 3D XY predictions for several materials but the disagreement concerning correlation-length anisotropy remains.

[4] H. K. M. Vithana, V. Surendranath, M. Lewis, A. Baldwin, K. Eidner, R. Mahmood, and D. L. Johnson, Phys. Rev. A **41**, 2031 (1990), and references therein.

[5] (a) D. Brisbin, R. DeHoff, T. Lockhart, and D. Johnson, Phys. Rev. Lett. **43**, 1171 (1979); (b) W. G. Bouwman and W. H. de Jeu, *ibid.* **68**, 800 (1992); in this work, the role of the splay elastic constant has been strongly emphasized in analysis of x-ray data; see, however, Ref. [3].

[6] J. L. Erickson, Arch. Ration. Mech. Anal. **4**, 231 (1960); **9**, 371 (1962); F. M. Leslie, Q. J. Mech. Appl. Math. **19**, 357 (1966); O. Parodi, J. Phys. (Paris) **31**, 581 (1970).

[7] Groupe d'Etude des Cristaux Liquids (ORSAY), J. Chem. Phys. **51**, 816 (1969).

[8] M. Miesowicz, Nature (London) **17**, 261 (1935); **158**, 27 (1946); Bull. Int. Acad. Pol. Sci. Lett. Cl. Sci. Math. Nat. Ser. A **228** (1936).

[9] J. Papánek, Mol. Cryst. Liq. Cryst. **179**, 139 (1990).

[10] G. Hu, H. Vithana, and D. L. Johnson (unpublished).

[11] A. Rapini and M. Papoular, J. Phys. (Paris) Colloq. **30**, C4-54 (1969).

[12] K. Eidner, M. Lewis, H. K. M. Vithana, and D. L. Johnson, Phys. Rev. A **40**, 6388 (1989).

[13] F. Jähnig and F. Brochard, J. Phys. (Paris) **35**, 301 (1974).

[14] P. Cladis and S. Torza, J. Appl. Phys. **46**, 584 (1975).

[15] C. Gooden, R. Mahmood, D. Brisbin, A. Baldwin, and D. L. Johnson, Phys. Rev. Lett. **54**, 1035 (1985).

[16] D. W. Allender, R. M. Hornreich, and D. L. Johnson, Phys. Rev. Lett. **59**, 2654 (1987).

[17] M. F. Achard, F. Hardouin, G. Sigaud, and H. Gasparoux, J. Chem. Phys. **65**, 1387 (1976).

[18] L. Chen, J. D. Brock, J. Huang, and S. Kumar, Phys. Rev. Lett. **67**, 2037 (1991).

[19] S. Sprunt, L. Solomon, and J. D. Litster, Phys. Rev. Lett. **53**, 1923 (1984).

[20] E. Gramsbergen and W. H. de Jeu, J. Chem. Soc. Faraday Trans. 2 **84**, 1015 (1988).

[21] The reference made in Ref. [18] to light-scattering measurements of ρ_3 for DHAOB and attributed to this group was incorrect.

[22] H. Vithana and D. Johnson (unpublished). The value of ρ_3 given for $\bar{6}09$ and the estimated error bars are based on the same kind and extent of analysis as that described here for DHAOB. Scanning force microscope studies of the sample substrates suggest that surface roughness plays an important role in explaining the difference between the FT and LS measurements of K_{33} for $\bar{6}09$.

[23] C. W. Garland, M. Meichle, B. M. Ocko, A. R. Kortan, C. R. Safinya, L. J. Yu, J. D. Litster, and R. J. Birgeneau, Phys. Rev. A **27**, 3234 (1983); C. R. Safinya, Ph.D. dissertation, MIT, 1981.

[24] B. Ocko, Ph.D. dissertation, MIT, 1984.

[25] We note that the growth of smectic order near the boundaries can explain the smallness and constancy of d_e in the asymptotic regime since one can show that $W_0 \sim \xi_\parallel$ due to the energy cost of tilting the director relative to the layers. This is a subtle issue, however, which we plan to discuss elsewhere.